Received: 11 December 2024 | Revised: 7 April 2025 | Accepted: 9 April 2025

DOI: 10.1002/esp.70067

RESEARCH ARTICLE

ESPL WILEY

Erosion dynamics in carbonate bedrock channels inhibit weathering processes

Elizabeth H. Dingle[1] | Edwin R. C. Baynes[2] | Alex Hall[1,2] | Jeff Warburton[1]

[1]Department of Geography, South Road, Durham University, Durham, UK

[2]Geography and Environment, Loughborough University, Loughborough, UK

Correspondence
Elizabeth H. Dingle, Department of Geography, South Road, Durham University, Durham, UK.
Email: elizabeth.dingle@durham.ac.uk

Funding information
Natural Environment Research Council (NERC), Grant/Award Number: NE/X017567/1; British Society for Geomorphology

Abstract

The interplay of rock weathering and erosion processes controls the erodibility of bedrock. Existing models of these processes in bedrock river channels have been developed using observations largely from silicate lithologies, neglecting the effects of the dissolution of soluble carbonate minerals. Here, we present a study of rock erodibility in two limestone bedrock channels in the North Pennines, UK. Patterns in rock erodibility were assessed using Schmidt hammer surveys conducted in 12 cross-sections and were analysed alongside calculations of bedrock inundation interval, observations of sediment transport from bedload impact plates and long-term estimates of limestone dissolution rates from environmental data. Results show that erosion via dissolution can result in similar patterns of rock erodibility observed in silicate channels where erosion outpaces weathering. Bedrock inundation interval is a key control on bedrock erodibility, although to a lesser degree than channels in silicate lithologies. Where the channel margin is not regularly inundated by flow, weathering processes which weaken the rock are still present but may be locally offset by dissolution driven by soil seepage of low pH runoff which erodes weathered material. Furthermore, we do not always observe the expected impacts of weathering and erosion on channel geometry, with channel geometry seemingly more sensitive to the availability of abrasive tools (sediment supply). Long-term estimates of abrasion and dissolution rate are broadly equivalent at our study site further demonstrating the effectiveness of dissolution at eroding carbonate lithologies, although further work is needed to isolate feedback between these two variables. Future studies of bedrock incision processes in carbonate landscapes should re-evaluate how mechanical erosion and dissolution are represented, and how sensitive the balance of these processes is to potential changes in inundation frequency and climate.

KEYWORDS
abrasion, bedrock erosion, dissolution, weathering

1 | INTRODUCTION

Bedrock channel incision rates are intrinsically linked to bedrock erodibility (e.g., Limaye & Lamb, 2014; Murphy et al., 2016; Sklar & Dietrich, 2001; Small et al., 2015). The rate at which bedrock channels vertically incise mediates how changes in boundary conditions (e.g., base-level, climate) are transmitted across landscapes, driving changes in hillslope erosion rate, hillslope-channel connectivity, valley geometry and downstream sediment supply (e.g., Brocard & van der Beek, 2006; Burbank et al., 1996; Giachetta et al., 2014; Hurst et al., 2013; Limaye & Lamb, 2014; Schlunegger et al., 2001; Whipple, 2004). Material properties of bedrock resist erosion and the erodibility of the rock can be directly related to measurements of tensile strength (e.g., Lamb et al., 2015; Scheingross et al., 2014; Sklar & Dietrich, 2001), compressive strength (e.g., Kent et al., 2020; Lifton et al., 2009; Murphy et al., 2016; Shobe et al., 2017), discontinuity spacing (e.g., Spotila et al., 2015) and mineral grain size (Larimer et al., 2022; Turowski et al., 2023).

Chemical and physical weathering processes can reduce rock tensile strength, making surfaces more susceptible to mechanical erosion by particle impacts (abrasion) and by removal of fracture-bound blocks of bedrock by hydraulic action (plucking) (e.g., Murphy et al., 2016). Here, we define weathering processes as those that contribute to the in-situ breakdown of rock, while erosion is defined as the dynamic removal of rock surface material. Bedrock is mechanically eroded when material is dislodged from the surface (abrasion and plucking), which can be aided through the development of coalescing micro-scale crack networks caused by accumulated damage from sediment impacts and chemical weathering (e.g., Chatanantavet & Parker, 2009; Larimer et al., 2022; Sklar & Dietrich, 2001). Additionally, bedrock surfaces may develop laterally extensive planes of weakness (e.g., along bedding planes) that facilitate the plucking of larger intact blocks during high-magnitude flows (e.g., Beer et al., 2017; Whipple et al., 2000). Chemical and physical weathering processes can also expand natural discontinuities in the rock surface (e.g., via freeze–thaw), and accelerate erosion through block plucking by shear flow even in the absence of bedload sediment transport (Lifton et al., 2009). Parts of the channel cross-section that are frequently inundated experience higher rates of mechanical erosion through bedrock abrasion and/or plucking, which modulates rock strength by removing weaker weathered material (Murphy et al., 2018), resulting in mechanically stronger surfaces that are characterised by low bedrock erodibility. Total erosion in this instance is set by the rate at which unweathered material is removed from bedrock surfaces by mechanical erosion. In this scenario, weathering rates could be described as kinetically-limited, as fresh mineral surfaces are exhumed faster than weathering fronts can develop (e.g., West et al., 2005).

Conversely, in parts of the channel cross-section that are infrequently inundated, weathering fronts have time to develop in the surficial few millimetres of the rock surface (e.g., Montgomery, 2004; Phillips et al., 2019), resulting in higher bedrock erodibility (Shobe et al., 2017). In sedimentary lithologies (e.g., sandstone, mudstone), surface weathering rind thickness has been shown to be less in continuously submerged parts of the channel, relative to bedrock valley faces which experience frequent cycles of wetting and drying (Montgomery, 2004). Johnson and Finnegan (2015) demonstrated that repeated cycles of wetting and drying can weaken bedrock bank material depending on the material properties of the bedrock. Weakened weathered or fractured rock may then be entrained or eroded by clear water flow (e.g., Howard, 1998). Because weathered material at the rock surface is less frequently removed on the channel margins, weathering rates may eventually be limited by the absence of fresh minerals being exhumed to the rock surface (i.e., mineral-supply limited weathering). Therefore, we expect that the relative balance of weathering and erosion should produce differences in bedrock erodibility around the channel perimeter.

Modelling studies exploring the effect of bedrock weathering on channel geometry and slope in response to variable discharge and erosion rate, have suggested that more erodible weathered channels (e.g., mineral supply-limited) are wider, deeper and less steep than non-weathered channels (e.g., kinetics-limited) all else being equal (Hancock et al., 2011). Field observations by Shobe et al. (2017) suggested that patterns of channel erodibility are driven by spatially variable erosion rates, which influence channel width-to-depth ratios through the relative balance of weathering and erosion on the channel thalweg and banks. Existing studies exploring the relative balance of in-channel weathering and erosion in bedrock channels have focused on catchments characterised by silicate-rich lithologies (e.g., Anderson et al., 2000 (metagreywacke, metapelites); West et al., 2005 (granitoid, felsic metapelites); Emberson et al., 2016 (schist, greywacke, argillite); Shobe et al., 2017 (schist, metagreywacke); Bufe et al., 2021, 2022 (shale, sandstone, granitoid)). To date, carbonate lithologies (e.g., limestone, dolomite) have largely been overlooked in landscape evolution studies despite them covering 10–12% of ice-free continental areas (Ford & Williams, 2007; Ott et al., 2019).

In carbonate landscapes, dissolution results in the simultaneous removal of soluble (e.g., calcite) and surrounding insoluble minerals from rock surfaces. In this sense, dissolution can contribute to bedrock erosion in carbonate channels and can occur in addition to mechanical erosional processes such as abrasion and plucking. However, dissolution can also be considered as a chemical weathering process. In the absence of flowing water (e.g., ponded water in bedrock depressions), in-situ weathering of bedrock surfaces may also occur at a very localised scale via the dissolution of soluble minerals. While the controls on mechanical erosion rates are relatively well-understood (e.g., the 'tools and cover' effect; Sklar & Dietrich, 2001), there is a lack of understanding of carbonate lithology dissolution rates, patterns of surface lowering by dissolution within a channel cross-section and the implications for the exposure of rock surfaces to weathering. Potential feedback between dissolution and mechanical erosion rates also remains largely unexplored at the channel reach scale. Calcite dissolution in 28 U.S. Geological Survey-monitored streams has been estimated to result in erosion rates in the order of a few tenths of a millimetre per year (Covington et al., 2015; Covington & Vaughn, 2019), which implies our current understanding of landscape evolution, driven purely by mechanical processes, may be missing a significant component of surface lowering in carbonate landscapes.

Here, we investigate the relationship between bedrock channel geometry and the distribution of rock erodibility where surface lowering is a function of weathering, dissolution and mechanical erosion. Using field evidence from channels incised into limestone, we assess the feedback between bedrock erosion, weathering and rock erodibility, applying the methodological framework of Shobe et al. (2017). We isolate the roles of abrasion and dissolution on rock erodibility and channel geometry by comparing two channels with contrasting bedload sediment supply but otherwise similar boundary conditions (e.g., lithology, climate, temperature) and calculate multi-decadal estimates of bedrock abrasion and dissolution rates using environmental data. This analysis specifically allows us to explore (1) patterns of bedrock erodibility in carbonate channels, (2) the role of bedload sediment supply and dissolution on carbonate bedrock erodibility and geometry and (3) how cross-sectional patterns of bedrock erodibility vary between carbonate and non-carbonate landscapes.

2 | STUDY SITE

The Moor House Bedrock River Observatory (MH-BRO) is located within the Moor House Upper Teesdale National Nature Reserve (North Pennines, UK; Figure 1a), which is an established research site for ecological and environmental monitoring and part of the UK Environmental Change Network. Within the MH-BRO site, we focus on two bedrock channel reaches, in the Trout Beck (drainage area of ~8 km^2) and Rough Sike (~1 km^2) mixed bedrock-alluvium catchments. Both channels are characterised by a flashy, temperate hydrological regime due to the high rainfall (annual total precipitation ~ 2000 mm yr-1; [Burt et al., 1998]) and extensive blanket peat, moorland land cover (Figure 2). During winter months, the region frequently experiences sub-zero (°C) temperatures and bedrock channel banks experience frequent cycles of freeze–thaw physical weathering (SI Figure S1). In both areas, channels are incised into the same underlying geological parent unit of interbedded Carboniferous limestone, sandstone and shale units (Johnson & Dunham, 1963; Figure 1b). The main study channels are formed in the Tynebottom Limestone member which consists of a blue-grey, thick-bedded, fossiliferous, stylolitic limestone with intercalated thin mudstone beds. The rocks are part of a structural unit known locally as the Alston Block, consisting of a comparatively stable area of basement rocks bounded by faults. The main strata dip gently in an east-north-easterly direction, approximately parallel to the Trout Beck stream, with mid-Pleistocene uplift rates estimated at 0.2 mm yr^{-1} and

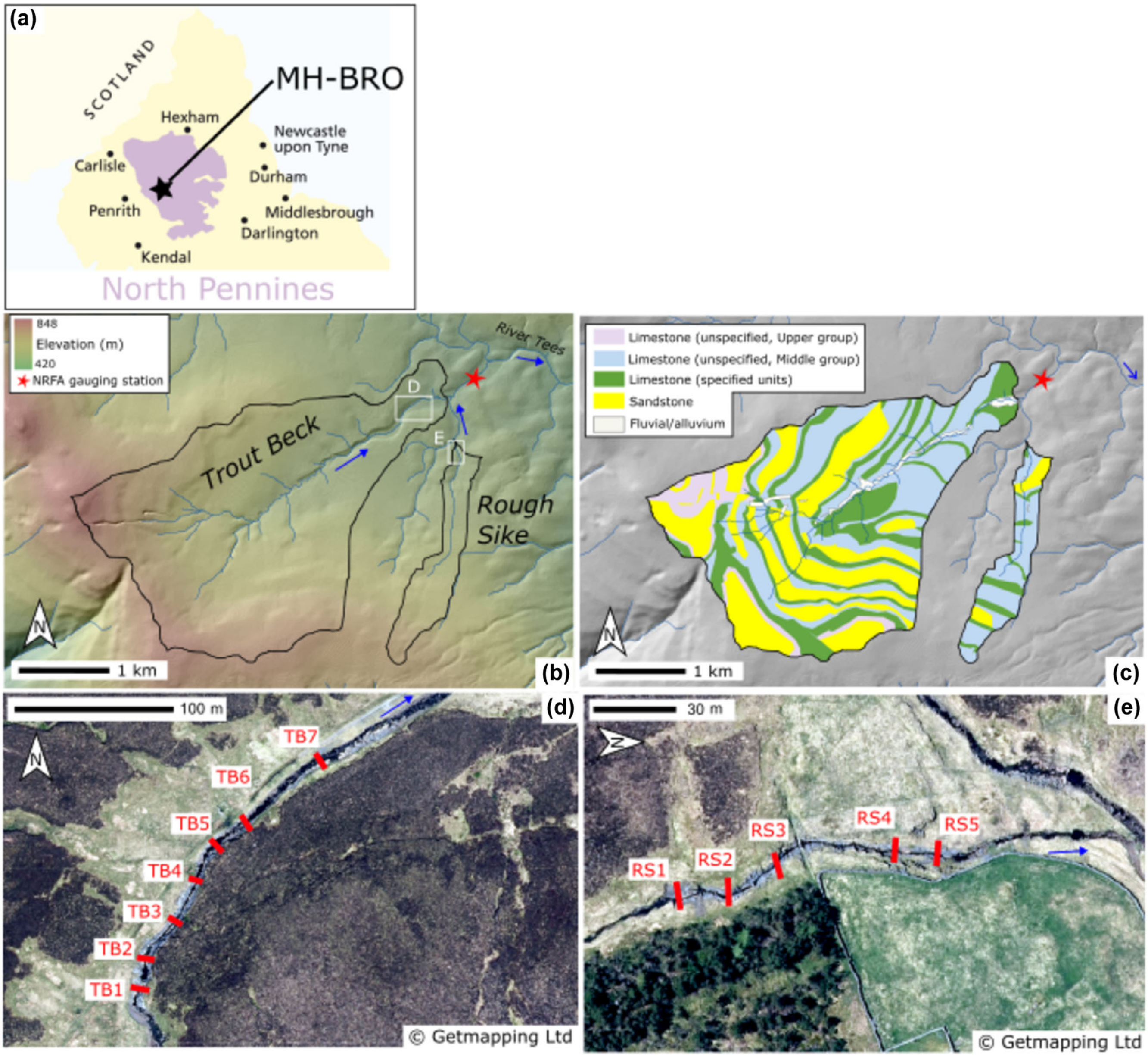

FIGURE 1 The moor house Bedrock River observatory (MH-BRO) study location. (a) The location of MH-BRO in the north Pennines natural landscape in northern England. (b) Digital elevation model and trout Beck and Rough Sike catchment outlines. Red star shows the location of the National River Flow Archive (NRFA) gauging station (station number 25003, grid reference NY757335). White boxes show the locations of the bedrock study reaches in each catchment (panels d and e). (c) Map of key lithologies within MH-BRO, digitised from Johnson and Dunham (1963). (d) Bedrock study reach in trout Beck, with cross-sections shown in red. (e) Bedrock study reach in Rough Sike, with cross-sections shown in red. aerial images in panels D and E are 0.25 m resolution, downloaded from Getmapping, using EDINA aerial Digimap service (accessed 7th March 2024).

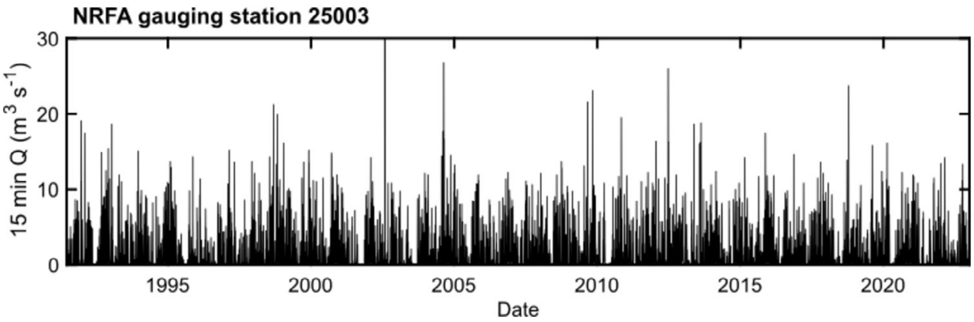

FIGURE 2 15-minute discharge record between 1991 and 2022 from the UK National River Flow Archive gauging station number 25003 'Trout Beck at Moor House' located ~300 m downstream of the confluence of trout Beck and Rough Sike (see Figure 1).

subsequently altered by glacio-isostatic adjustment and erosion. Present-day estimates of crustal movement (i.e., uplift or subsidence) are negligible for the region (e.g., Shennan, 1989).

Carbonate dissolution microtopography (karren, scallops) is abundant along the perimeter of the channels, where dissolution can be driven by acidic runoff and seepage from the adjacent blanket peat, as well as flow in the active channel. In the lower channel, local microtopography is also generated by abrasion and pothole formation processes. During the low flow, planar bedrock surfaces (benches) are exposed across much of the channel bed, ~0.1 to 0.3 m above the channel thalweg, which is incised into a narrower 'low flow' channel (> 1 m wide). Where seepage collects within depressions in bedrock microtopography (i.e., it is not freely flowing), bedrock can appear highly weathered at a very localised scale. Both channels are approximately rectangular, and their banks are largely composed of horizontal/sub-horizontal bedded limestone units of 0.1 to 0.7 m thickness, with channel bank heights ranging from 0.8 to 2 m. Channels at Trout Beck are typically wider (~4–6 m) than at Rough Sike (~2–4 m) which reflects the contrast in upstream drainage areas. Blanket peat, typically varying between 1 and 2 m in depth, fringes both channels and delivers acidic runoff to the channel margin. The streamflow pH of both Rough Sike and Trout Beck typically varies between 4.7–7.1 and 5.3–8.1, respectively, where pH is negatively correlated with discharge in both channels highlighting the acidic nature of the blanket peat-dominated catchment hydrology (SI Figure S2).

Despite the proximity of the channels to one another, we hypothesize that the relative importance of weathering, dissolution and mechanical erosion in Rough Sike and Trout Beck is likely to differ because sediment supply (from incised glaciofluvial deposits beneath the peat) has largely been evacuated from the Rough Sike channel and banks. As such, dissolution is hypothesized to set patterns of rock erodibility in Rough Sike. In contrast, the larger Trout Beck system has ample coarse sediment supply that is frequently mobilised by high flow events (Ferguson, Sharma, Hardy, et al., 2017), and there is widespread evidence of bedrock abrasion and plucking on the channel bed (Figures 3 and 4). As such, both dissolution and mechanical erosion are hypothesised to set patterns of bedrock erodibility and channel geometry in Trout Beck. Bedload is typically comprised of sub-rounded to rounded sandstone and limestone particles varying in size up to ~200 mm (e.g., Ferguson, Sharma, Hodge, et al., 2017) that are widespread in alluvial cover upstream of the bedrock reach (Figure 1b). While sediment cover on the bed of the channel may inhibit or reduce potential bedrock dissolution rates (e.g., Covington et al., 2015), the bedrock reach on Trout Beck is largely free of persistent sediment cover which should maximise potential abrasion rates during peak flow events. We therefore anticipate that erosion may outpace weathering at Trout Beck, resulting in narrower and steeper channels with more uniform patterns of rock erodibility (e.g., Hancocket al., 2011).

3 | METHODS

3.1 | Morphological analysis – cross-section surveys

Channel cross-sections were measured at Rough Sike and Trout Beck (five and seven sites, respectively; Figures 1, 3, and 4) to characterise channel reach morphology and locate Schmidt hammer surveys. Cross-sections were surveyed using a tape measure and metre staff, while also noting the distribution of vertically aligned dissolution features and limestone bedding planes on the banks. Water surface slope (*S*) was calculated during low flow conditions using an EMLID Reach RS + RTK GPS with survey accuracy of ±0.02 m, down a stream length equivalent to ~5–10 channel widths (Table 1).

At Rough Sike, cross-section 1 (RS1) is situated between two ~1 m vertical knickpoints, one of which is associated with a mineral vein. RS2, RS3 and RS4 are located downstream of the mineral vein in a confined bedrock gorge (Figure 3a–d). RS5 is located at the distal end of the confined bedrock reach, before the channel transitions into a mixed alluvial-bedrock reach (Figure 3e). Small patches of fine gravel are present on the bed upstream of RS1, and coarser sediment and boulders occur on the bed downstream of RS5 but are rare within the bedrock gorge. At Trout Beck, TB1 is located downstream of an alluvial reach characterised by relatively coarse grain sizes (D_{50} = 36 mm, D_{84} = 116 mm; Ferguson, Sharma, Hodge, et al., 2017) and is immediately upstream of the primary waterfall (~2 m high) (Figure 4a) which is incised in the main limestone unit but does not appear to correspond to any obvious lithological contact. TB2 to TB5 are within the confined bedrock gorge (Figure 4b–e). TB6 is at the downstream limit of the gorge, where the channel is starting to become unconfined (Figure 4f). At TB7, the channel is mixed bedrock-alluvial, and laterally unconfined on the right bank (Figure 4g). Sediment cover in the channel is highly variable. TB1 is virtually sediment-free. Sediment is often evident within the low flow portion of the channel in TB2 to TB5 (0–40%) with nearly full bed coverage at TB6 (ranging in size from fine gravel to boulder) (Figure 4). Section TB7 is bounded by alluvial channel banks with gravel sediment in the low-flow channel (covering approximately 10–20% of the bed).

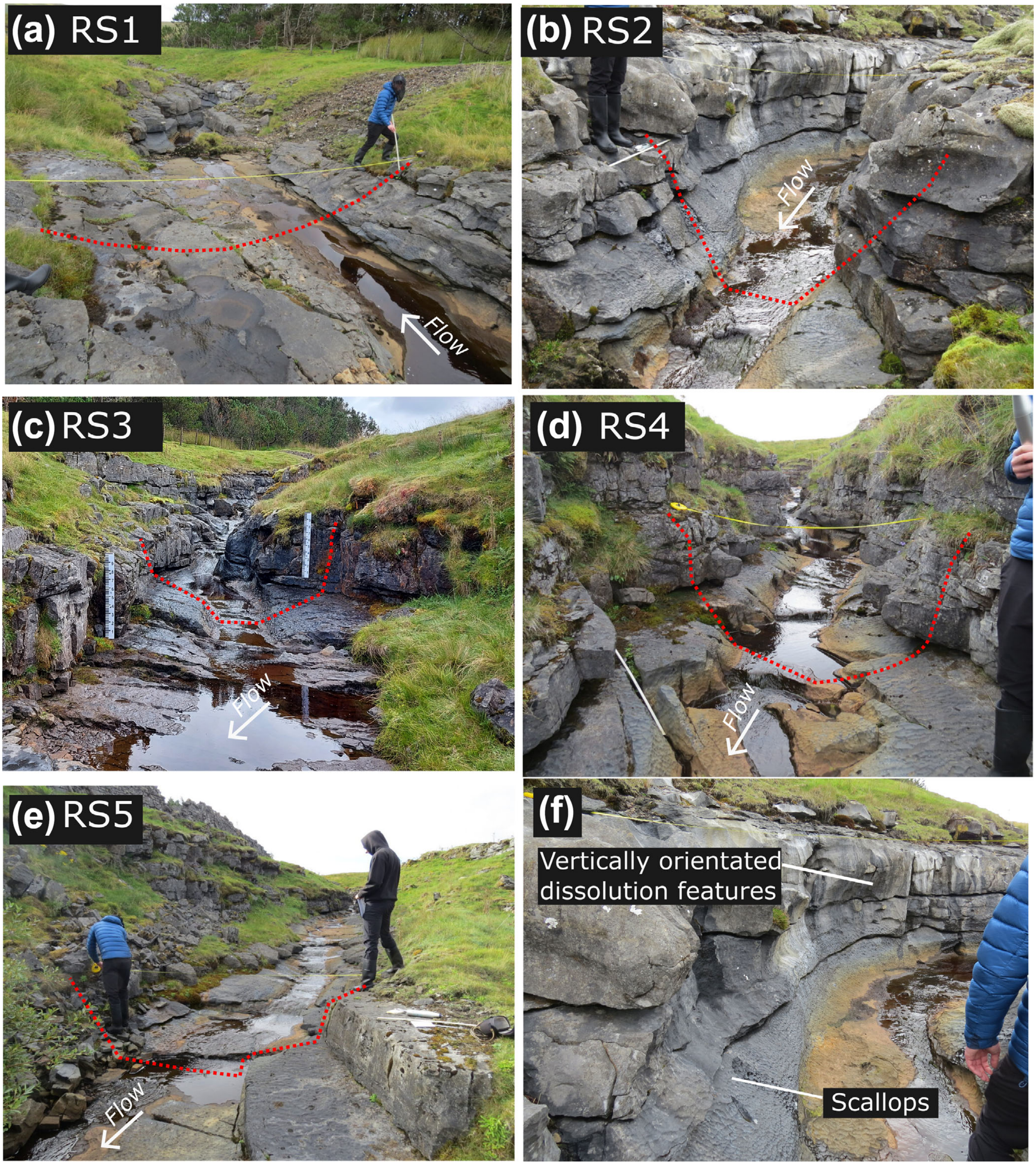

FIGURE 3 (a)–(e) Cross-sections on rough Sike from upstream to downstream (RS1 to RS5), (f) distribution of vertically aligned dissolution features at top of bank face, and scallops present near the channel bed.

3.2 | Schmidt hammer surveys

To characterise rock erodibility, compressive strength measurements were taken using an N-type Schmidt hammer (Viles et al., 2011). The Schmidt hammer does not provide a direct measure of uniaxial compressive rock strength, but rather a proprietary unit of compressive strength, *Q*, which corresponds to the rebound velocity of the hammer on striking the rock surface (Aydin, 2015). Higher Schmidt hammer values reflect greater rock compressive strength and have been used extensively to explore spatial patterns of weathering rates and processes (e.g., Larimer et al., 2022; Nicholson, 2008, 2009). Estimates of rock uniaxial compressive strength have also been made from Schmidt hammer rebound data from a range of rock types (e.g., Morales et al., 2004) and correlate with point load data.

At least six evenly spaced vertical sets of 25 Schmidt hammer measurements were collected between the channel thalweg and bank top (Table 1), on vertical rock surfaces that were free of vegetation. We did not sample on especially uneven or fractured surfaces where

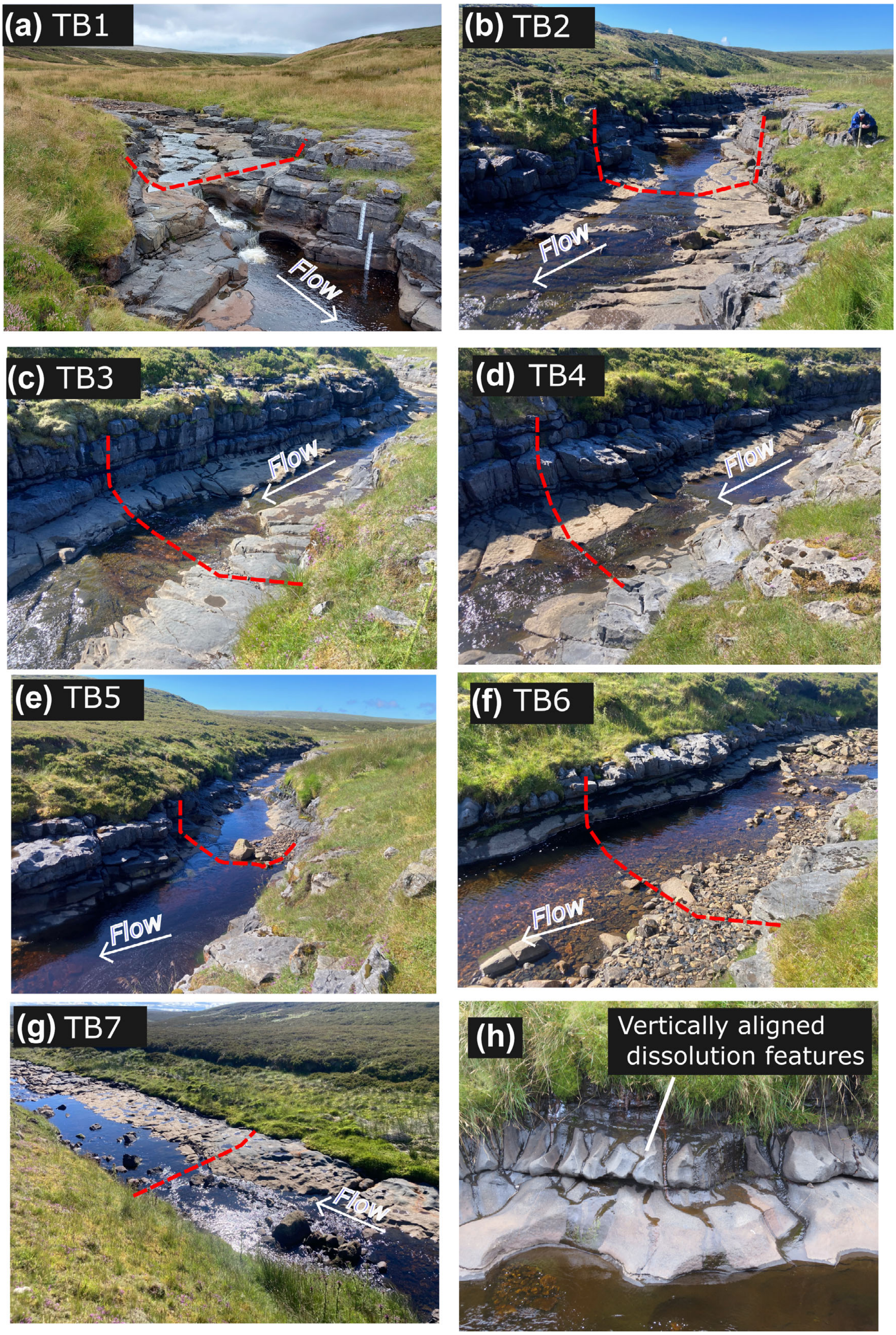

FIGURE 4 (a)–(g) Cross-sections on trout Beck from upstream to downstream (TB1 to TB7), (h) shows vertically aligned dissolution features (rillenkarren) beneath overhanging blanket peat.

the Schmidt hammer may not return accurate rebound values (e.g., Aydin, 2015). At TB7, where the banks are largely alluvial, measurements were restricted to the exposed bedrock bed (Figure 4). In the confined bedrock reaches, we did not include the uppermost section of banks if there were clearly imprinted by vertical dissolution features (e.g., Figures 3f and 4h), formed by bank-top seepage from adjacent blanket peat. A separate dataset assessing for differences in Schmidt hammer value on horizontal and vertical surfaces was also

TABLE 1 Cross-section characteristics and sampling details.

Cross-section ID	Low flow water surface slope (m/m)*	Number of Schmidt samples	Description
RS1	0.022	150	Low gradient, semi-confined
RS2	0.082	150	High gradient, confined
RS3	0.048	150	Intermediate gradient, confined
RS4	0.069	150	High gradient, confined
RS5	0.015	150	Low gradient, semi-confined
TB1	0.041	175	Top of waterfall, semi-confined
TB2	0.002	150	End of plunge-pool, wide, confined, low gradient
TB3	0.028	150	High gradient, confined
TB4	0.019	150	High gradient, confined
TB5	0.017	150	High gradient, confined
TB6	0.016	150	Intermediate gradient, confined
TB7	0.011	150	Low gradient, unconfined

*Elevation data used to calculate slope values were within ±0.02 m vertical accuracy.

collected to test for systematic differences that may arise through hammer angle (see Supporting Information).

3.3 | Bedrock inundation interval and stream power calculations

Bedrock inundation intervals (i.e., a measure of how often parts of the bedrock bank are inundated) were calculated using flow-frequency analysis of 15-minute interval discharge data available from the Environment Agency Trout Beck gauging station (1991–2022; Figure 2). To calculate flow-frequency statistics on each channel, data from the Trout Beck gauging station were scaled by upstream catchment areas for the Trout Beck and Rough Sike study reaches. Previous work on Trout Beck has suggested a near 1:1 fit between measured and scaled discharges using catchment area ratios, and in lieu of directly measured discharges we assume this area ratio approach can be similarly applied to Rough Sike given the comparable catchment characteristics and proximity (Sharma, 2016). As there are no significant tributaries entering either study reach, we assumed that discharge should not vary substantially between cross-sections, so a single discharge scaling was used on each channel based on the contributing drainage area of the most upstream cross-section. The overall change in catchment area between the most upstream and downstream cross-sections was 1.1% and 1.4% on Rough Sike and Trout Beck, respectively, supporting our approach.

A Gumbel distribution was fitted to the 32-year of scaled maximum annual flow measurement data to calculate flow-frequency statistics for both study reaches. Using the cross-section profiles and the flow-frequency analysis, a discharge rating curve was created at each cross-section. Cross-sectional area with height above the thalweg was measured at 5 cm vertical intervals and multiplied by the cross-sectional mean flow velocity from Manning's equation to calculate discharge (Q_w) at each 5 cm interval. Each 5 cm interval corresponded to <0.1 m^3 s^{-1} of Q_w, so where inundation levels fell between increments, we rounded to the nearest 5 cm. We justify this approach owing to the relatively small impact this would have on calculated inundation interval relative to errors generated by the simplification of cross-sectional geometry. We used the measured low-flow water surface slope (S) at each site (Table 1). Manning's n has previously been calculated for a range of discharges in Trout Beck and reduces with increasing Q_w from ~0.09 to 0.2 when Q_w < 1 m^3 s^{-1}, to values of ~0.04–0.08 when 1 > Q_w > 10 m^3 s^{-1} (Ferguson, Sharma, Hardy, et al., 2017). There is considerable variability in the absolute values of n between ~100 m long reaches on Trout Beck, so it is difficult to ascribe a single value of n relative to Q_w. In our calculations of Q_w, we simplify Manning's n to a representative value of 0.07 based on observations made by Ferguson, Sharma, Hardy, et al. (2017), and because the inundation interval statistics we use represent discharges > 1 m^3 s^{-1}. The calculated Q_w at each stage interval was then compared to the flow-frequency analysis to calculate the inundation depths and channel widths of the 2-year (Q_2), 10-year (Q_{10}) and 50-year (Q_{50}) inundation interval discharges. The approximate channel width (w) of the Q_{10} discharges were also measured from the cross-section profiles.

Shobe et al. (2017) suggested that gradients of rock compressive strength should increase with erosion rate. Their study location spanned between the Potomac River and Piedmont province, where 10^3–10^6 yr erosion rates differ by an order of magnitude due to a migrating knickzone. By assuming a simple linear extrapolation in erosion rate between these two regions, Shobe et al. (2017) used unit stream power (Ω) as a proxy for erosion rate in the absence of direct measurements. Given the post-orogenic nature of our study site, we would expect erosion rates to be uniformly low across MH-BRO. However, we test for spatial variability in Ω to explore possible drivers in patterns of bedrock erodibility. We calculate Ω using the Q_{10} flow statistic at each cross-section where:

$$\Omega = \frac{\rho g Q_w S}{w} \tag{1}$$

where ρ = fluid density (kg m^{-3}) and g = gravitational acceleration (m s^{-2}).

3.4 | Long-term abrasion rate estimates

To quantify the potential effectiveness of mechanical erosion (by saltation-abrasion) in Trout Beck, we use the 15-minute gauged flow record (1991–2022) and bedload impact plate data from our study reach in a modified version of the saltation-abrasion model. The saltation-abrasion model was originally developed for quantifying erosion rates (E) produced by abrasion of planar bedrock surfaces by saltating sediment particles (Sklar & Dietrich, 2004) where:

$$E = V_i I_r F_e \tag{2}$$

where V_i is the volume of rock eroded per particle impact, I_r is the particle impact rate per unit area and F_e is the fraction of the bed exposed to streamflow. In Trout Beck, we assume that F_e is equal to 1 owing to a general lack of persistent sediment cover. The V_i parameter in Equation 2 can also be approximated using the vertical component of particle impact velocity onto the channel bed (ω_{si}) where:

$$V_i = \frac{\pi \rho_s D_s^3 \omega_{si}^2 Y}{6 k_v \sigma_T^2} \tag{3}$$

where ρ_s is the density of sediment (2,650 kg m^{-3}), D_s is the grain diameter (assumed to be D_{50}), Y is Young's modulus of elasticity, k_v is a dimensionless abrasion coefficient and σ_T is the tensile yield stress of bedrock. Because direct measurements of ω_{si} (in Equation 3) were not included in their original model, Sklar and Dietrich (2004) also suggested that a mean sediment particle descent velocity (ω_{sd}) can be written as:

$$\omega_{sd} = 0.4 (R_b g D_s)^{\frac{1}{2}} \left(\frac{\tau^*}{\tau_c^*} - 1 \right)^{0.18} \tag{4}$$

where R_b is the nondimensional buoyant density of sediment ($\frac{\rho_s}{\rho_w} - 1$), τ^* is the dimensionless Shield's number and τ_c^* is the critical Shield's number. Sklar and Dietrich (2004) proposed that on average, the vertical velocity attained when a particle reaches the same elevation as take-off (on a planar surface) is approximately twice that of ω_{sd}. This allows ω_{si} in Equation 3 to be approximated by ω_{sd} derived in Equation 4 where:

$$\omega_{si} \sim 2\omega_{sd} \tag{5}$$

Sharma (2016) presented bedload impact rate data collected using two 15 cm × 13 cm × 0.6 cm impact plates installed flush on the bed of Trout Beck proximal to our cross-sections TB2 and TB7. The sensors consisted of an accelerometer connected to a metal plate, that was mounted onto the river bed, with a maximum sensor sensitivity of 1 impact per 0.2 seconds and saturation value of 255 impacts per 5 minutes. Power-law relations were fitted between bedload impacts per 5-minute interval (I) and Q_w for a series of high-flow events documented over a 20-month period between September 2013 and April 2015 by Sharma (2016). An average relation was also fitted to data across all high-flow events recorded at both impact plates. These average relations assume a critical value of Q_w (Q_{crit}) above which appreciable bedload impacts were recorded (i.e., >50 counts per 5 minutes). We apply the average I- Q_w relation and Q_{crit} for each impact plate across the full Q_w record for Trout Beck to generate a timeseries of bedload impacts at 15-minute intervals. Some of the individual bedload transport events reported in Sharma (2016) revealed evidence of sediment supply limitations (i.e., hysteresis) which introduces uncertainty in our approach. Similarly, Q_{crit} varied between individual sediment transport events. We can account for the uncertainty in Q_{crit} by using both the Q_{crit} value averaged over the full event timeseries, and the highest Q_{crit} calculated for an individual storm event to provide a more conservative abrasion rate estimate.

Using 15-minute gauged Q_w data (Figure 2), we calculated the number of bedload particle impacts per 15 minutes of the Q_w record as:

$$I = 72(Q_w - 2.5)^{1.8} \tag{6}$$

for Q_w measurements in excess of Q_{crit} = 4.0 m^3 s^{-1} for the impact plates near TB2, and 4.1 m^3 s^{-1} near TB7, as noted by Sharma (2016). We also estimate impacts for maximum Q_{crit} values of 6.0 and 5.8 m^3 s^{-1}, for plates at TB2 and TB7 respectively. Estimates of τ^*(Equation 7) were also made using relations between Q_w and bed shear stress (τ) calculated for high-flow stages on Trout Beck at TB2 (Equation 8) and at TB7 (Equation 9) (Sharma, 2016) where:

$$\tau^* = \frac{\tau}{(\rho_s - \rho_w) g D_s} \tag{7}$$

$$\tau = 43.4 {Q_w}^{0.61} \tag{8}$$

$$\tau = 32.5 {Q_w}^{0.49} \tag{9}$$

Estimates of E (Equation 1) were made for each 15-minute increment of Q_w where bedload particle impacts were detected, and summed to create a cumulative erosion rate. In the model, a regional limestone σ_T of 6.4 MPa was used based on values reported by Attewell (1971), which varied from 1.6 to 6.4 MPa in northern England. A Young's elastic modulus of 38 GPa was also applied (e.g., for stylotitic limestones; Al-Shayea, 2004). While Sklar and Dietrich (2004) originally proposed values of k_v of the order of $\sim 10^6$, values of k_v have been reported to be closer to $\sim 10^5$ for materials with tensile strength greater than 1 MPa (Auel et al., 2017) which is consistent with our values for σ_T. We assume a value of 0.045 for τ_c^* which is widely accepted for gravel bed rivers, and a characteristic grain size of 63 mm as reported by Sharma (2016). The original saltation-abrasion model was designed to be applied to planar bedrock surfaces, excluding the effects of bed topography on kinetic energy transfer to the bed (Huda & Small, 2014). Through the inclusion of uneven bedrock surfaces, Huda and Small (2014) and Larimer et al. (2021) suggested that erosion may be orders of magnitude larger than for an equivalent plane bed. For low transport stages (where the dimensionless transport stage (τ^*/τ_c^*) < 1) modelled erosion was estimated to be ~10 times greater in uneven bedrock surfaces, and more than 100 times greater at high transport stages (τ^*/τ_c^* > 4). We calculate a range of possible event-scale abrasion rates for planar bedrock surfaces (lower estimate) and uneven bedrock surfaces at average transport stages where bedload motion is detected in appreciable quantities (upper estimate).

3.5 | Long-term limestone dissolution rates

Point sampling of surface water pH, temperature and calcium concentrations are available for Trout Beck (at the NRFA gauging station - weekly) and Rough Sike (monthly) from the UK Environmental Change Network (ECN) stream water chemistry dataset (Rennie et al., 2017). In total, 177 (Rough Sike) and 534 (Trout Beck) point samples between 1997 and 2011 were available with concurrent measurements for all three variables. We use concurrent timeseries of all three parameters in the *olm (v. 0.39)* python package (Covington et al., 2015) to produce a timeseries of dissolution rate for both systems. The Trout Beck data set was collected downstream of the confluence with Rough Sike, so we are unable to isolate the dissolution rate specifically on the Trout Beck study reach itself. We implemented the *palmerFromSolution()* function for impure calcite which uses the Palmer (1991) dissolution equation, which is more representative of dissolution rates observed in typical limestone bedrock (e.g., Covington & Vaughn, 2019). Within the *palmerfromSolution()* function, the partial pressure of CO_2 is calculated from pH, calcium concentration and water temperature using the *solutionfrompHCaRelaxed()* function, which assumes an open H_20-CO_2-$CaCO_3$ system. This approach assumes that dissolution rates are surface reaction rate limited, however, Covington and Vaughn (2019) found good agreement between independently measured dissolution rates and those calculated with the *olm* package.

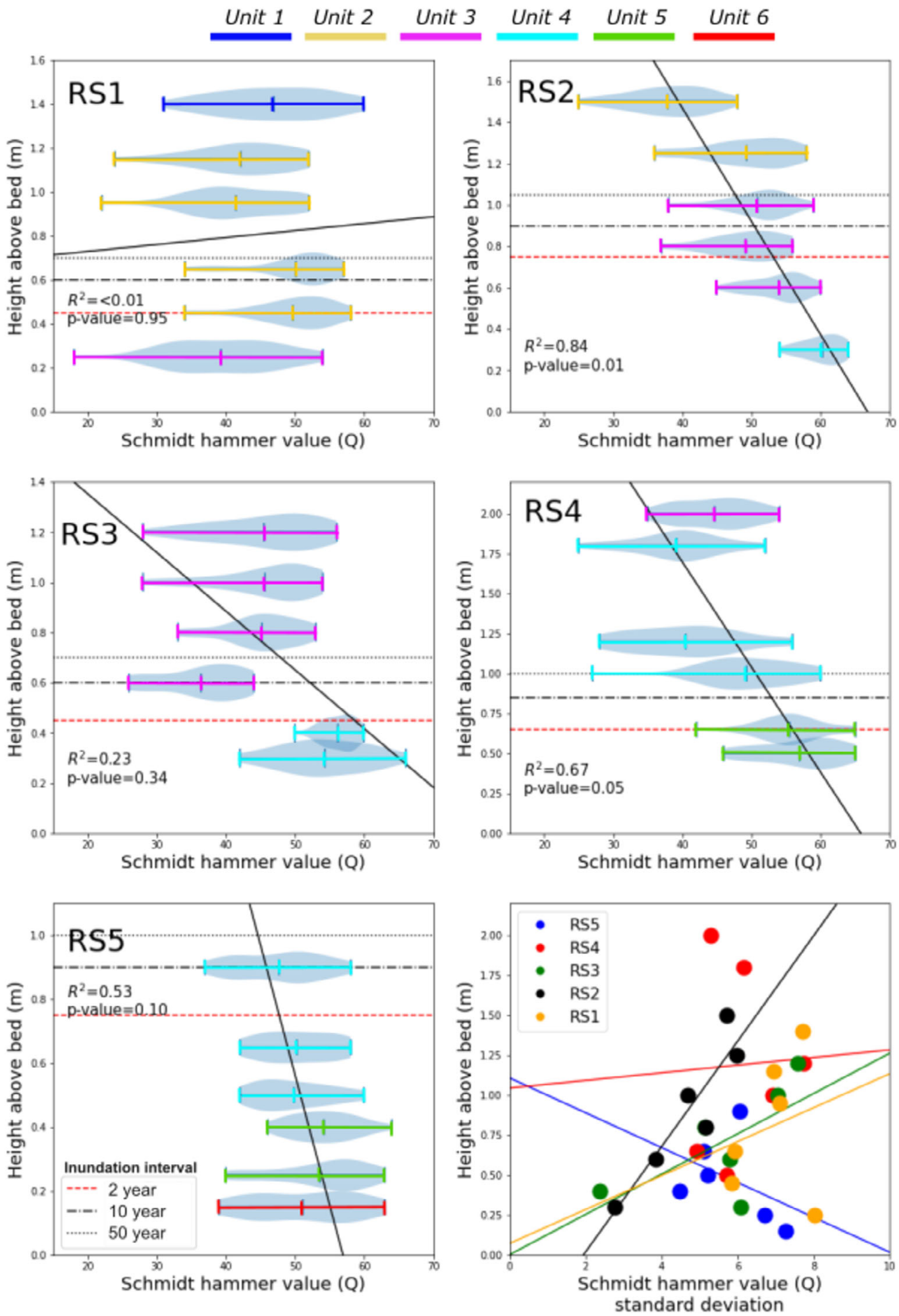

FIGURE 5 Schmidt hammer values and standard deviation against height above bed and in relation to inundation levels for rough Sike. Units 1–6 represent contiguous limestone units exposed along the study reach. The local geological units shown here do not correlate to those shown for trout Beck (Figure 6). Regression lines in the lower right panel are coloured according to the colour scheme for each transect shown in the legend.

4 | RESULTS

4.1 | Compressive rock strength variability at the cross-section scale

In four of the five cross-sections at Rough Sike (RS2–RS5), compressive strength decreases with height above the channel bed (Figure 5). The degree of scatter varies between individual sites, but in sites RS2 and RS4, there are statistically significant relations between compressive strength and height above the channel bed (p-value <0.05, >95% confidence) (Table 2). In RS1, there is no relation between compressive strength and height above the channel bed, with the lowest mean Schmidt hammer value recorded closest to the bed (Figure 5). At RS2 and RS3 the standard deviation of Schmidt hammer values increases with height above the channel bed (Figure 5), with smaller increases in standard deviation noted in RS1 and RS4 with increasing height. At RS5, there is a slight decrease in Schmidt hammer value standard deviation with height above the channel bed. At RS2 and RS4 where the channel has the lowest width-to-depth ratio (1.8 and 1.7, respectively), there is a significant relation between height and compressive strength (p-value < 0.05). The gradient of rock compressive strength (i.e., the slope of the best-fit relation between Schmidt hammer value and height above the bed) at each cross-section varies from −0.4 (RS1) to 15.4 (RS2) where larger gradients reflect greater differences in rock strength at the channel bed and bank top (Table 2), and negative values represent lower Schmidt hammer values at the bed relative to the bank top. Where the same bedding unit is present at multiple cross sections, Schmidt hammer values generally vary and other than RS1, the highest Schmidt hammer values (>60 Q) are located closest to the bed regardless of the bedding unit. This suggests that local variability in Schmidt hammer values is driven by weathering/erosion processes rather than the material properties (e.g., mineral composition) of each bedding unit. At RS3, there is a clearer contrast in Schmidt hammer values between Unit 3 and Unit 4 which may be due to local variability in rock properties.

In Trout Beck, rock compressive strength decreases with height above the bed but there is considerable scatter in the data (Figure 6). At TB3 and TB5, there are significant relations between Schmidt hammer value and height above the bed (p-value <0.05, confidence >95%) (Table 2), but this relation appears independent of either channel geometry or unit stream power. In contrast, at TB4 and TB7 there is no relation between Schmidt hammer value and height (Table 2), where bed and bank top average values are within the error range of each other. The standard deviation in the Schmidt hammer value at each height also varies between cross-sections, and with height above the bed (Figure 6), but generally standard deviation in the Schmidt hammer value increases with height above the channel bed (Figure 6). At TB7 the channel was unconfined, limiting Schmidt hammer measurements to the exposed bed of the channel which is fully inundated by the 2-year inundation interval discharge. Schmidt hammer values are notably uniform ranging from 56 to 59 Q and with low standard deviation (<4 Q). The gradient of rock compressive strength at each cross-section on Trout Beck varies from 1.2 (TB4) to 13.3 (TB1) (Table 2), suggesting that the channel bed is typically characterised by lower rock erodibility (i.e., greater compressive strength) than the bank top. Like Rough Sike, individual bedding units are characterised by a range of Schmidt hammer values between cross-sections, although there is a strong contrast between Unit 1 and Unit 2 at TB1 (Figure 6). Unit 4 is generally characterised by higher Schmidt hammer values in TB3–7, but is present at the base of all cross-sections where rock strength would be expected to be greatest (see SI Figure S3).

4.2 | Compressive rock strength and bedrock inundation interval

At RS1-RS4, the channel contains the 50-year interval discharge (2.9 $m^3\ s^{-1}$; Table 3), but the 50-year interval discharge is overbank at the distal downstream site (RS5) where the channel is no longer fully confined by high bedrock banks (Figure 5). At RS2, RS3 and RS4 there

TABLE 2 Lowest (near bed) and highest (near bank top) height Schmidt hammer value measurements, and p-values between height and Schmidt hammer value at each cross-section. Shaded cells have a p-value of ≤ 0.05.

Cross-section ID	Schmidt hammer value (Q) at lowest sample (± 2 x SD)	Mean Schmidt hammer value (Q) (± 2 x SD)	Schmidt hammer value (Q) at highest sample (± 2 x SD)	Height above bed and Schmidt hammer p-value	Height above bed and Schmidt hammer r^2
			Rough Sike		
RS1	39 ± 16	45 ± 16	47 ± 15	0.95	<0.01
RS2	60 ± 5	50 ± 16	38 ± 11	0.01	0.84
RS3	54 ± 12	47 ± 18	45 ± 15	0.34	0.23
RS4	57 ± 11	48 ± 19	45 ± 11	0.05	0.67
RS5	51 ± 15	51 ± 13	48 ± 12	0.10	0.53
			Trout Beck		
TB1	50 ± 9	50 ± 22	42 ± 17	0.06	0.54
TB2	52 ± 11	49 ± 16	43 ± 17	0.08	0.58
TB3	57 ± 5	52 ± 16	47 ± 14	0.02	0.79
TB4	56 ± 5	52 ± 17	51 ± 11	0.88	0.01
TB5	57 ± 5	54 ± 13	45 ± 11	0.03	0.73
TB6	55 ± 9	52 ± 13	50 ± 13	0.07	0.60
TB7	49 ± 7	58 ± 5	57 ± 4	0.43	0.16

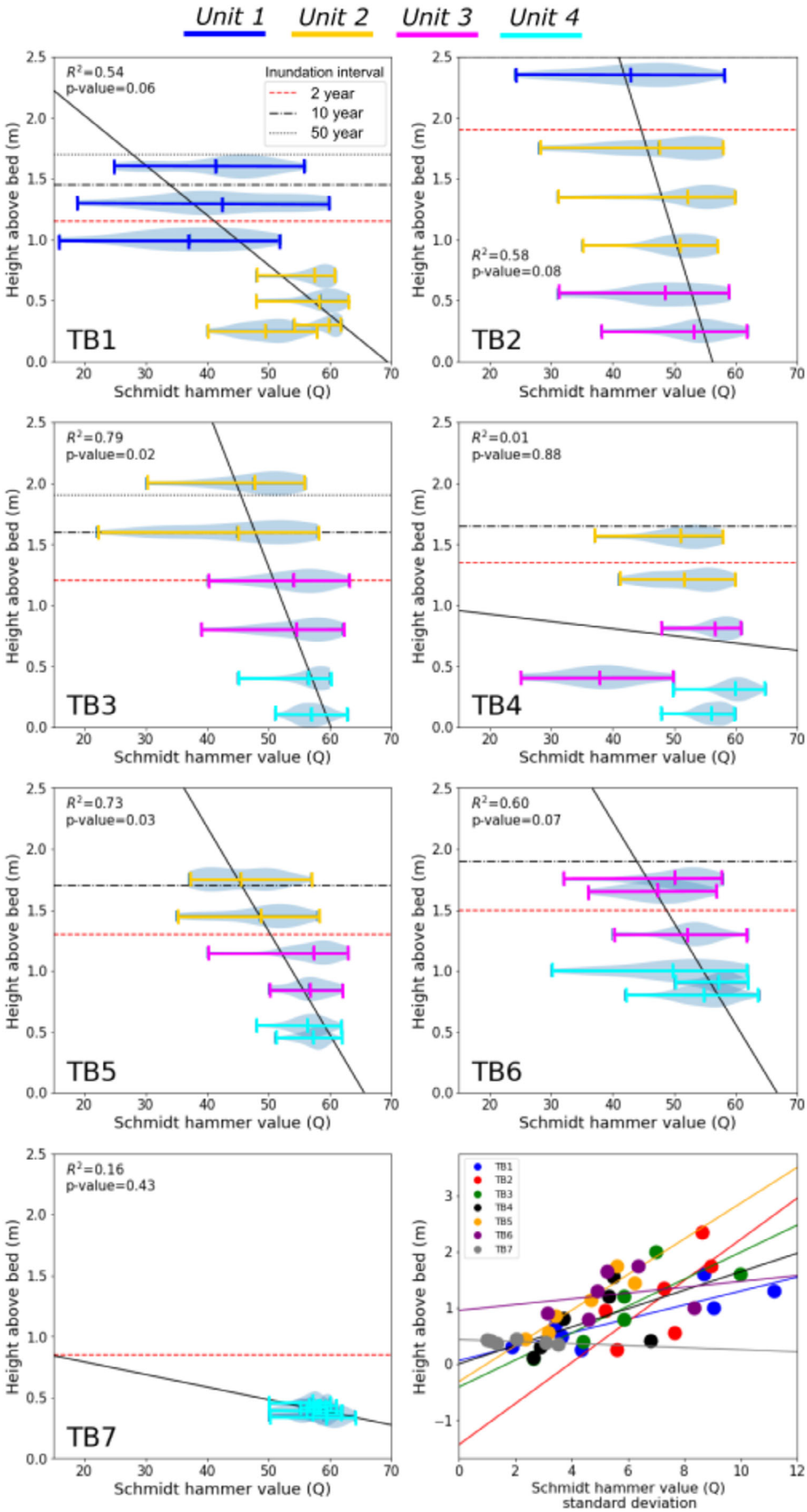

FIGURE 6 Schmidt hammer measurements and standard deviations against height above bed and in relation to 2- and 10-year inundation levels for trout Beck. Units 1–4 represent contiguous limestone units exposed along the study reach. The local geological units shown here do not correlate to those shown for rough Sike (Figure 5). Regression lines in the lower right panel are coloured according to the colour scheme for each transect shown in the legend.

TABLE 3 Bedrock inundation discharges for 2-, 10- and 50-year intervals on trout Beck and Rough Sike.

Inundation interval	Trout Beck	Rough Sike
Q_2	9.5 m^3 s^{-1}	1.3 m^3 s^{-1}
Q_{10}	15.6 m^3 s^{-1}	2.1 m^3 s^{-1}
Q_{50}	21.6 m^3 s^{-1}	2.9 m^3 s^{-1}

is a general increase in compressive rock strength with decreasing inundation interval, but values are largely within the error range of each other (±2 SD). At Trout Beck, the channel only typically contains the 2- to 10-year interval discharges (9.5 and 15.6 m^3 s^{-1}, respectively; Table 3) before going overbank (Figure 6). At TB3, the capacity of the bedrock reach is slightly larger and can contain the 50-year interval discharge (21.6 m^3 s^{-1}).

There is a statistically significant relation between Schmidt hammer value and bedrock inundation interval at both Trout Beck and Rough Sike, with Spearman correlation coefficients (ρ) of −0.60 and −0.65, respectively, and p-values of <0.0005 (Figure 7). This is comparable with observations made in silicate-dominated terrain by Shobe et al. (2017), which showed similar values of correlation and significance (−0.71 and <0.0001, respectively). Schmidt hammer values in Trout Beck and Rough Sike do not reduce with increasing bedrock inundation interval to the same degree as noted in Shobe et al. (2017), with mean Schmidt hammer values for >10-year interval discharges remaining largely above 40 *Q* in Trout Beck and Rough Sike, while dropping below 20 *Q* in Virginia. This may in part relate to the limited number of measurements with inundation intervals greater than 50 years in Trout Beck, as these discharges were out of the channel.

In Rough Sike, the channel width-to-depth ratio varies between 1.7 and 5.0 for the 10-year inundation interval discharge, while Ω varies between 57 (RS5) and 706 W m^{-2} (RS2) (Table 4). There is a negative correlation between channel width-to-depth ratio and Ω on Rough Sike which is significant at >99% confidence (r^2 = 0.96, p-value <0.01). There is a weak positive correlation between Ω and the gradient of rock compressive strength (r^2 = 0.66, p-value = 0.09) at Rough Sike (Figure 8b), and no relation between the gradient of rock compressive strength and channel width-to-depth ratio (r^2 = 0.46, p-value = 0.21) (Table 4). In Trout Beck, the channel width-to-depth ratio is less variable ranging from 2.94 (TB2) to 5.66 (TB1), while Ω ranges from 47 W m^{-2} (TB2) to 754 W m^{-2} (TB1) (Figure 8a). There is no correlation between Ω and channel width-to-depth ratio (r^2 = 0.37, p-value = 0.20), between Ω and the gradient of rock compressive strength (r^2 = 0.28, p-value = 0.28), or channel width to depth ratio and the gradient of rock compressive strength (r^2 = 0.46, p-value = 0.14) at Trout Beck (Table 4). For a given value of Ω, the gradient of rock compressive strength is generally higher in Rough Sike than in Trout Beck (Figure 8b). As Ω increases, the channel width-to-depth ratio tends to increase in Trout Beck but decreases in Rough Sike (Figure 8a).

4.3 | Long-term abrasion estimates

Over the 32-year discharge record, potential cumulative erosion (by abrasion) varies between 9.6 and 13.7 mm at Trout Beck (0.3–0.4 mm yr^{-1}) (Figure 9). Using the more conservative Q_{crit} value yields lower erosion of 6.9–9.0 mm (0.2–0.3 mm yr^{-1}). The average dimensionless transport stage (τ^*/τ_c^*) during which substantial bedload impacts were observed was 2.6 at the upstream impact plate (at TB2) and 1.6 at the downstream impact plate (at TB7). Accounting for variations in bed topography and transport stage (Huda & Small, 2014), we place an upper limit on potential erosion rates by abrasion at 2.2–4.3 mm yr^{-1} (∼ 10 times the solution for a planar bed, based on the average dimensionless transport stage and Q_{crit}).

4.4 | Long-term dissolution rate estimates

Dissolution rates varied between 0 and 7.0 mm yr^{-1} with long-term averages of 0.98 mm yr^{-1} and 0.58 mm yr^{-1} at Rough Sike and Trout Beck, respectively (Figure 10). These rates are generally quite high in comparison to other limestone channels (e.g., Covington et al., 2015; Covington & Vaughn, 2019) but we attribute this to the relatively low pH of surface waters which will facilitate faster rates of dissolution (e.g., Alkattan et al., 1998). This also reflects the higher dissolution rate in Rough Sike, which is likely caused by the lower average pH in Rough Sike over Trout Beck. These dissolution rates are consistent with observations in Alaska, where runoff from acidic peat bogs has produced dissolution rates of up to 1.66 mm yr^{-1} (Allred, 2004). Ten samples in the Trout Beck record (<2% of total samples) produced no dissolution, which we attribute to supersaturation with respect to calcite owing to high pH values on these days (pH > ∼8).

5 | DISCUSSION

5.1 | What sets how bedrock erodibility is distributed in carbonate channels?

5.1.1 | Rough Sike (dissolution dominated erosion)

Patterns of bedrock erodibility have been shown to be sensitive to erosion rate, however, at MH-BRO we expect uniform rates of erosion as crustal movement and fault activity at MH-BRO are negligible (e.g., Shennan, 1989). This may explain the general lack of relations between Ω and channel width-to-depth ratio and gradient of rock compressive strength (Figure 8). However, we still find a statistical correlation between Ω and the gradient of rock compressive strength at Rough Sike. It has been suggested that a weak scaling (1/3 to 1/2 power) between dissolution rate and flow shear stress exists, where dissolution rates are controlled by mass transport rather than just surface reaction rate (Covington et al., 2015; Opdyke et al., 1987). Owing to the lack of readily available sediment to mechanically abrade the bed in Rough Sike, the higher values of rock compressive strength found near the bed at RS2-RS4 may reflect higher Ω, which facilitates higher rates of carbonate dissolution than at RS1 and RS5 for a given discharge (Table 4). Higher rates of dissolution should promote the removal of weakened bedrock surface material and yield a higher rock compressive strength, which is consistent with our observations at Rough Sike. However, we cannot neglect the influence of mechanical erosion by plucking along the channel margins. Field observations

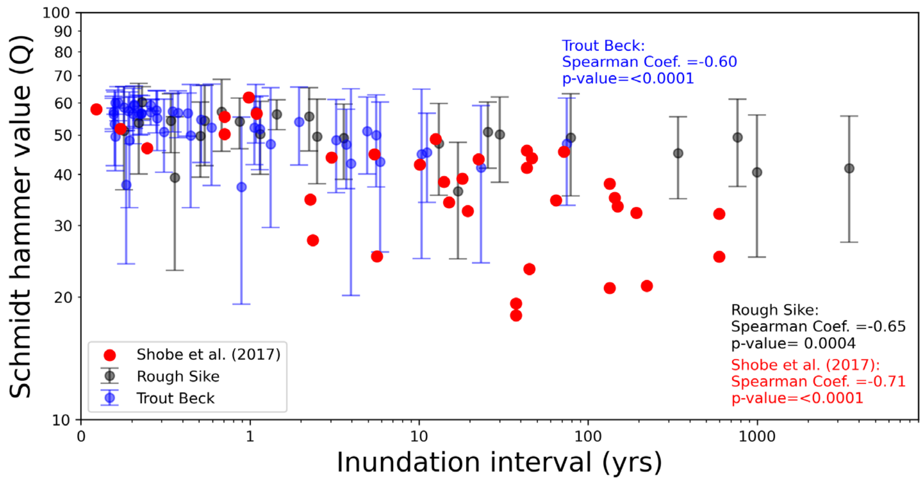

FIGURE 7 Comparison of Schmidt hammer value and inundation interval in carbonate and non-carbonate (from Shobe et al., 2017: shown in red) landscapes. Spearman correlation coefficients (ρ) and p-values are given for trout Beck and Rough Sike, and as reported for channels in Shobe et al. (2017). Error-values for Shobe et al. (2017) data are not reported here for figure clarity but are available in the original citation.

TABLE 4 Unit stream power and channel width to depth ratios for 10-year inundation interval discharges, and gradient of compressive rock strength at each cross-section.

Cross-section ID	10 yr unit stream power (USP) (W m^{-2})	10 yr width/depth ratio (WDR)	Gradient of compressive strength (GCS)	WDR and USP	GCS and USP	GCS and WDR
Rough Sike (RS)						
RS1	*109*	*4.0*	*−0.4*	$R^2 = 0.96$ *p-value = 0.004*	$R^2 = 0.66$ *p-value = 0.09*	$R^2 = 0.46$ *p-value = 0.21*
RS2	*706*	*1.8*	*15.4*			
RS3	*328*	*3.4*	*9.9*			
RS4	*651*	*1.7*	*10.2*			
RS5	*57*	*5.0*	*6.6*			
Trout Beck (TB)						
TB1	*754*	*5.7*	*13.3*	$R^2 = 0.37$ *p-value = 0.20*	$R^2 = 0.28$ *p-value = 0.28*	$R^2 = 0.46$ *p-value = 0.14*
TB2	*47*	*2.9*	*3.8*			
TB3	*789*	*3.4*	*6.1*			
TB4	*426*	*3.9*	*1.2*			
TB5	*411*	*3.5*	*8.8*			
TB6	*385*	*3.4*	*6.8*			
TB7	-	-	-			

indicate mechanical erosion by block plucking is likely to be minimal on the active channel bed, which appears largely polished (Figure 3). Plucking is more evident on channel banks which often appear more blocky (Figure 3b). Theoretically, this should lead to a strengthening of the banks relative to the bed (if erosion and weathering by dissolution were not important), however, we see the reverse (Figure 5). The absence of large detached blocks of limestone in and downstream of the Rough Sike study reach suggests that plucking is perhaps only relevant during very exceptional flows and over long timescales. We therefore expect patterns of rock erodibility to reflect the shorter-term balance of weathering and dissolution.

Bedrock inundation interval also appears to influence gradients of compressive strength to some degree. RS5 has a relatively low gradient of compressive strength while still having relatively high Schmidt hammer values at both bed and bank top samples. This may to attributable to a difference in channel geometry and capacity, where the channel can only contain the 2-year inundation interval discharge at RS5, which should aid in the mechanical removal of weathered or weakened rock surfaces by shear flow at a higher elevation due to the more frequent inundation (Howard, 1998; Johnson & Finnegan, 2015; Montgomery, 2004).

5.1.2 | Trout Beck (dissolution and mechanical erosion)

The relation between rock compressive strength and Ω is less clear on Trout Beck, where bedrock inundation interval seems to have a stronger control on patterns of erodibility. Cross-sections with the highest near-bed Schmidt hammer values correspond to high Ω, but gradients of rock compressive strength are poorly correlated to Ω with considerable variability over a narrow range of Ω. The lower gradients of rock compressive strength and the higher average Schmidt hammer values in Trout Beck over Rough Sike reflect the greater inundation frequency in Trout Beck, where the Trout Beck channel can typically only contain the 2- to 10-year inundation interval discharge. Greater

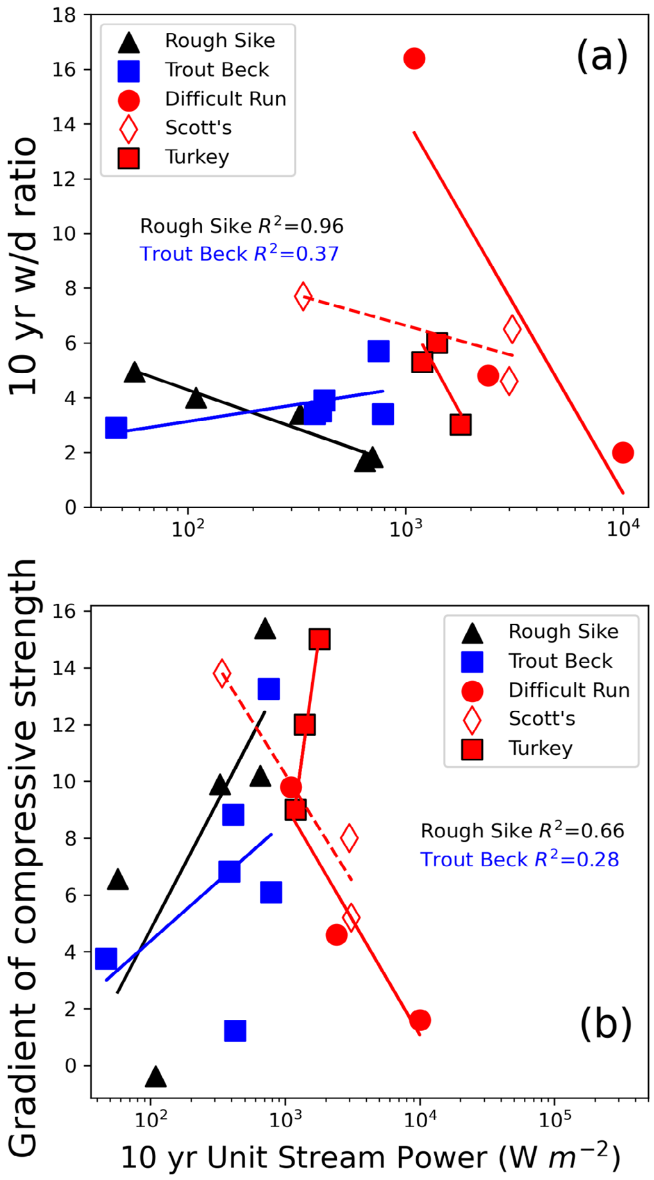

FIGURE 8 (a) Channel geometry and unit stream power in rough Sike and trout Beck, (b) unit stream power and gradient of rock compressive strength in channel banks of rough Sike and trout Beck. Published data from non-carbonate sites in Shobe et al. (2017) are shown in red. Additional analysis removing data points TB4, RS1 and RS3 are also shown in Figure S4 and Table S1 as these are sites where no or very weak correlation between rock compressive strength and height above bed were noted.

inundation frequency promotes the removal of weathered or damaged rock surfaces on the channel banks (e.g., Montgomery, 2004). Unlike Rough Sike, we find evidence of active plucking such as sub-angular blocks of limestone on the channel bed at Trout Beck, which would be facilitated by more frequent channel inundating flows. When low bedrock inundation intervals are combined with mechanical erosion by plucking and abrasion, higher rock compressive strengths can be maintained around the channel boundary at Trout Beck resulting in lower gradients of compressive strength for a given value of Ω than observed in Rough Sike (Figure 8b). As such, we hypothesise that gradients of compressive rock strength are sensitive to the low bedrock inundation interval at Trout Beck, which is enabled by the relatively small capacity of the bedrock channel and the flashy catchment discharge regime. Unlike Rough Sike, there is limited time for weathering fronts to develop in the bedrock surface of the banks at Trout Beck between high flow events, meaning bedrock incision is more closely linked to erosion by both dissolution and mechanical processes. This is consistent with earlier studies in that where erosion outpaces weathering, bedrock should be stronger with lower gradients of compressive strength (e.g., Hancock et al., 2011; Shobe et al., 2017).

5.2 | What effect does bedload sediment supply and dissolution have on carbonate bedrock erodibility and channel geometry?

Bedload sediment supply appears to affect both bedrock erodibility and channel geometry. Maximum Schmidt hammer values are comparable between Rough Sike and Trout Beck, possibly indicating the maximum strength of unweathered carbonate units across the study area. The greater variability in near-bed Schmidt hammer values (and higher standard deviations) at Rough Sike (Figure 5) may indicate that dissolution does not erode damaged bedrock surfaces as effectively or uniformly as where mechanical erosion by bedload transport is also present. Greater variability in Schmidt hammer values at Rough Sike could also reflect smaller scale variations in bedrock composition between limestone sub-units across sampling sites.

Width-depth ratios at Rough Sike are often lower than at Trout Beck which could suggest that erosion is outpacing weathering at Rough Sike to a greater degree. However, we find that channel geometry is poorly correlated to patterns of rock erodibility. For channels that experience both dissolution and mechanical erosion (e.g., Trout Beck), we suggest that the dominant processes controlling the width-depth ratio is more likely some combination of higher rates of bank material plucking (Spotila et al., 2015) and the presence of bedload supply rather than the weathering impact on rock erodibility. Increasing bedload sediment supply has been shown to cause widening of bedrock channels (e.g., Baynes et al., 2020; Buckley et al., 2024; Finnegan et al., 2007; Li et al., 2023; Yanites & Tucker, 2010), by widening the band of active sediment transport along exposed bedrock channel beds until sediment cover starts to develop on the channel bed. Similarly, higher rates of bank plucking facilitated by more frequent channel inundating flows would contribute to channel widening. At MH-BRO, we would therefore expect to see wider channels with mechanically stronger beds at Trout Beck than Rough Sike for all else being equal owing to mechanical erosion.

At Rough Sike, we might anticipate that the total erosion rate would be lower than at Trout Beck owing to the lack of bedload supply. This is supported by the lower gradients of compressive strength observed at Trout Beck than Rough Sike for a given value of Ω. Our estimates of the potential abrasion rate along Trout Beck suggest mechanical erosion could be highly effective. The greatest source of uncertainty in the potential abrasion rate estimates is accounting for bed topography during high transport stages, which increases the calculated abrasion rate by an order of magnitude. The model also assumes that saltating particles are of an equivalent lithology to the impacted bedrock surface. At Trout Beck, much of the available bedload supply entering the limestone bedrock reach is sandstone gravels, cobbles and small boulders which visually appear quite

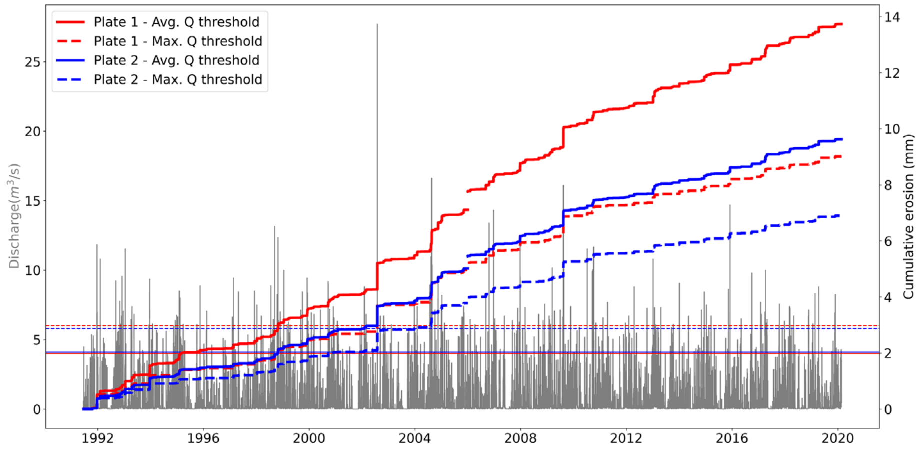

FIGURE 9 Time-series of discharge (grey), and potential cumulative erosion (by abrasion) for upstream (red) and downstream (blue) impact plate data. Estimates using the average (solid line) and maximum (dashed line) Q_{crit} thresholds are shown for both sets of data. Average abrasion rates (mm yr^{-1}) are shown by the red and blue horizontal lines.

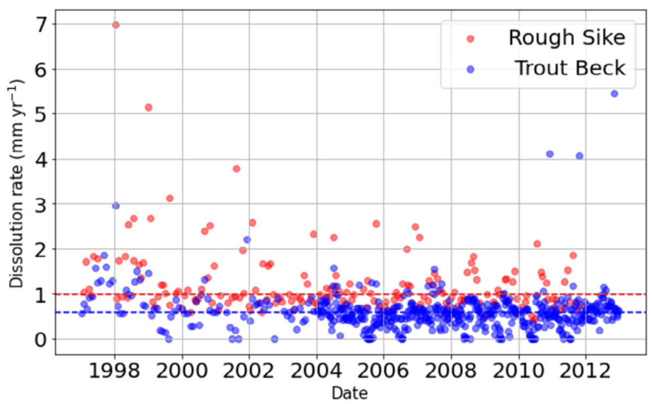

FIGURE 10 Timeseries of dissolution rate estimates on trout Beck (blue) and rough Sike (red), with the 15-year average value shown by dashed lines.

weathered (and edge-rounded). The tensile strength of sandstone is typically lower than limestone and would be further reduced if weathered. As such, total abrasion by sandstone particles impacting a mechanically stronger limestone bedrock surface is likely to be lower than for equivalent limestone particles (e.g., Attal & Lavé, 2009; Fox et al., 2023).

Importantly, evidence of dissolution is widespread at Trout Beck despite high abrasion potential, where small patches of dissolution features such as scallops are present (SI Figure S5). Our time-series of dissolution rate suggests that surface lowering via dissolution can be a continuous process that can be active for as long as the unsaturated flow is present in the channel and yield comparable decadal-averaged erosion rates to abrasion. For a region that is tectonically quiescent, our first-order erosion estimates are >1 mm yr^{-1} which seems high. There are also outstanding questions regarding how dissolution rate impacts the volume of bedrock detached during individual particle collisions by saltating bedload. More research is needed to better understand how dissolution and abrasion interact and collectively erode bedrock. Without longer-term monitoring studies of bedrock incision rates (e.g., erosion pins, surface change detection), it is difficult to apportion the relative contributions of dissolution, saltation-abrasion and plucking to total bedrock incision rates at Trout Beck. Yet, given the contrast in bedload sediment supply between Rough Sike and existing studies (Shobe et al., 2017), we can infer that limestone dissolution yields comparable gradients in compressive rock strength to those produced by mechanical erosion of bedrock surfaces.

5.3 | How do cross-sectional patterns of bedrock erodibility compare between carbonate and non-carbonate landscapes?

The patterns of bedrock erodibility in this study and that of Shobe et al. (2017) appear remarkably similar, although may be a result of equifinality due to the variable erosion processes at work in carbonate and silicate landscapes (e.g., Covington et al., 2015) (Figure 10). Similar to earlier studies, bedrock inundation interval plays an important role in setting cross-sectional patterns of bedrock erodibility in limestone channels. Patterns in compressive rock strength and inundation interval appear to diverge in Rough Sike and channels in Virginia (Shobe et al., 2017). Samples from Rough Sike do not lose compressive strength as rapidly at higher inundation intervals in comparison to samples in Virginia which may be an effect of limited sampling at high bedrock inundation intervals at Rough Sike (Figure 7). Alternatively, this divergence could be explained by bank top and face dissolution driven by bank seepage from blanket peat set back from the bank top in Rough Sike that could result in the removal of weathered material in comparison to silicate lithologies that would likely just weather in-situ. The widespread presence of vertically aligned dissolution features on the upper banks of Rough Sike (Figure 3) is indicative of bank runoff being persistent, suggesting that upper bank surfaces may be experiencing some degree of dissolution irrespective of in-channel flow, which may locally strengthen or weaken the bank face depending on how effectively seepage removes weathered material from the bedrock surface. This interaction of in-situ weathering (e.g., freeze–thaw) and seepage may also produce higher gradients of rock compressive strength at Rough Sike, where the channel is also rarely completely inundated. If channels did not experience seepage, we may expect a stronger weathering signal in the upper banks (above Q_{50}), yielding cross-sectional patterns of rock erodibility that are more similar to a silicate-dominated landscape with lower rates of erosion. Similarly, if the channel on Trout Beck was larger capacity, we might expect to see a stronger signal of weathering on the upper bank where bedrock is less frequently inundated.

All else being equal, Hancock et al. (2011) predicted that channels should be wider, deeper and less steep in slower-eroding landscapes where weathering is allowed to increase rock erodibility. At MH-BRO we would expect to see relatively low rates of erosion and expect weathering processes to have an influence on patterns of rock erodibility, yet we find comparable gradients of rock compressive strength to those in Shobe et al. (2017) across erosion rates that ranged from ~0.1 m/kyr to >0.8 m/kyr. This suggests that erosional processes may be outpacing weathering at MH-BRO, which is consistent with our observations more generally. Interestingly, we find that relations between gradients of compressive strength and Ω are not fully consistent with patterns observed by Shobe et al. (2017), where we see increases in the gradient of compressive strength with Ω rather than decreases (Figure 8b). One interpretation of this relation reversal is due to scale effects, where Ω between the two studies varies by an order of magnitude and we may not be representing dynamics in larger catchments. Alternatively, given sites at MH-BRO should be eroding at a uniform rate, variations in Ω may simply arise from localised variability in limestone mineralogy and erodibility. Where bedrock is locally stronger, channel geometry may adjust and produce higher Ω. This is consistent with sites at Rough Sike where we observe a strong correlation ($r^2 = 0.96$) between Ω and width to depth ratio (Table 4). Elevated Ω should promote an increase in dissolution rate at the channel bed (sensu Opdyke et al., 1987). This could result in an increase in the gradient of compressive strength, such as we observe at Rough Sike in particular, where the channel margins are also much less frequently inundated than Trout Beck.

Dissolution is a key erosional process in carbonate channels that has implications for accurately modelling landscape evolution, where dissolution can maintain low erodibility surfaces within channels in the absence of mechanical erosion. While our observations at Rough Sike and, to a lesser degree, Trout Beck represent end-member scenarios (e.g., low pH, limited bedload supply), we have used this to specifically isolate the effects of bedload sediment supply and dissolution on rock erodibility. How well our findings map onto larger carbonate systems with different climatic regimes and environmental conditions (e.g., streamflow pH, mineralogy, tectonic setting), requires further investigation.

6 | CONCLUSIONS

Bedrock erosion processes in carbonate channels can produce comparable gradients of compressive rock strength to those in silicate channels characterised by high erosion rates, which we hypothesise is due to the dissolution of soluble minerals in the wetted perimeter of the channel. Dissolution, particularly in sections of the channel that are regularly inundated, limits the development of deep weathering profiles in carbonate rocks, leading to a lower gradient of compressive rock strength between the channel bed and the top of the banks. At the top of channel banks which are not regularly inundated by flow, weathering processes which act to weaken the rock are still present in carbonate channels but do not always generate the expected wider and deeper channel geometries that we would expect according to existing weathering-channel geometry models. We attribute this to the enhanced removal of weathered material by bank-top seepage. We find that mechanical erosion by abrasion is the dominant control on bedrock geometry, rather than patterns of bedrock erodibility. Collectively, our findings suggest that dissolution is potentially as important as mechanical erosion (saltation-abrasion) for controlling rates and patterns of weathering and erosion within bedrock channels. Given the extent of carbonate lithologies in continental land masses, future studies of bedrock channel incision processes should re-evaluate how mechanical erosion and dissolution are represented or parameterised, and how sensitive the balance of these erosional processes are to potential changes in flood and channel inundation frequency.

AUTHOR CONTRIBUTIONS

ED, EB and JW conceptualized the study and acquired funding. ED, EB and AH collected and analysed data and produced figures. ED and EB wrote the initial draft with inputs from AH and JW.

ACKNOWLEDGEMENTS

The authors thank Charlie Shobe for helpful comments that improved the initial manuscript and added clarity on our comparison to earlier studies. We also thank two anonymous reviewers for constructive and thought-provoking comments that improved the manuscript. EB, ED and JW acknowledge funding from the British Society for Geomorphology for supporting the Moor House Bedrock River Observatory, and the Upper Teesdale National Nature Reserve for continued access to the Moor House field site. ED was funded by a Natural Environment Research Council (NERC) Independent Research Fellowship (NE/X017567/1) and AH was funded by a NERC Centa Research Experience Placement. We thank Fiona Clubb for her assistance with fieldwork.

CONFLICT OF INTEREST STATEMENT

The authors have no conflicts of interest.

DATA AVAILABILITY STATEMENT

All data used in this manuscript are available within the manuscript and Supporting Information. Surface water chemistry and temperature data are available for Trout Beck and Rough Sike through the ECN Network (10.5285/fd7ca5ef-460a-463c-ad2b-5ad48bb4e22e).

ORCID

Edwin R. C. Baynes https://orcid.org/0000-0002-8666-7628
Alex Hall https://orcid.org/0009-0004-8857-7222

REFERENCES

Alkattan, M., Oelkers, E.H., Dandurand, J.-L. & Schott, J. (1998) An experimental study of calcite and limestone dissolution rates as a function of pH from −1 to 3 and temperature from 25 to 80°C. *Chemical Geology*, 151(1-4), 199–214. Available from: https://doi.org/10.1016/S0009-2541(98)00080-1

Allred, K. (2004) Some carbonate erosion rates of Southeast Alaska. *Journal of Cave and Karst Studies*, 66(3), 89–97.

Al-Shayea, N.A. (2004) Effects of testing methods and conditions on the elastic properties of limestone rock. *Engineering Geology*, 74(1-2), 139–156. Available from: https://doi.org/10.1016/j.enggeo.2004.03.007

Anderson, S.P., Drever, J.I., Frost, C.D. & Holden, P. (2000) Chemical weathering in the foreland of a retreating glacier. *Geochimica et Cosmochimica Acta*, 64(7), 1173–1189. Available from: https://doi.org/10.1016/S0016-7037(99)00358-0

Attal, M. & Lavé, J. (2009) Pebble abrasion during fluvial transport: experimental results and implications for the evolution of the sediment load along rivers. *Journal of Geophysical Research - Earth Surface*, 114(F4), F04023. Available from: https://doi.org/10.1029/2009JF001328

Attewell, P.B. (1971) Geotechnical properties of the great limestone in northern England. *Engineering Geology*, 5(2), 89–116. Available from: https://doi.org/10.1016/0013-7952(71)90014-7

Auel, C., Albayrak, I., Sumi, T. & Boes, R.M. (2017) Sediment transport in high-speed flows over a fixed bed: 2. Particle impacts and abrasion prediction. *Earth Surface Processes and Landforms*, 42(9), 1384–1396. Available from: https://doi.org/10.1002/esp.4132

Aydin, A. (2015) ISRM Suggested Method for Determination of the Schmidt Hammer Rebound Hardness: Revised Version. In: Ulusay, R. (Ed.) *The ISRM suggested methods for rock characterization, testing and monitoring: 2007–2014*. Cham: Springer International Publishing, pp. 25–33 https://doi.org/10.1007/978-3-319-07713-0_2

Baynes, E.R.C., Lague, D., Steer, P., Bonnet, S. & Illien, L. (2020) Sediment flux-driven channel geometry adjustment of bedrock and mixed gravel–bedrock rivers. *Earth Surface Processes and Landforms*, 45(14), 3714–3731. Available from: https://doi.org/10.1002/esp.4996

Beer, A.R., Turowski, J.M. & Kirchner, J.W. (2017) Spatial patterns of erosion in a bedrock gorge. *Journal of Geophysical Research - Earth Surface*, 122(1), 191–214. Available from: https://doi.org/10.1002/2016JF003850

Brocard, G.Y. & van der Beek, P.A. (2006) Influence of incision rate, rock strength, and bedload supply on bedrock river gradients and valley-flat widths: Field-based evidence and calibrations from western Alpine rivers (southeast France). In: Willett, S.D., Hovius, N., Brandon, M.T. & Fisher, D.M. (Eds.) *Tectonics, climate, and landscape evolution*, Vol. 398. Boulder, CO: Geological Society of America. Available from: https://doi.org/10.1130/2006.2398(07)

Buckley, J., Hodge, R.A. & Slater, L.J. (2024) Bedrock rivers are steep but not narrow: hydrological and lithological controls on river geometry across the USA. *Geology*, 52(7), 522–526. Available from: https://doi.org/10.1130/G51627.1

Bufe, A., Cook, K.L., Galy, A., Wittmann, H. & Hovius, N. (2022) The effect of lithology on the relationship between denudation rate and chemical weathering pathways – evidence from the eastern Tibetan plateau. *Earth Surface Dynamics*, 10(3), 513–530. Available from: https://doi.org/10.5194/esurf-10-513-2022

Bufe, A., Hovius, N., Emberson, R., Rugenstein, J.K.C., Galy, A., Hassenruck-Gudipati, H.J., et al. (2021) Co-variation of silicate, carbonate and sulfide weathering drives CO2 release with erosion. *Nature Geoscience*, 14(4), 211–216. Available from: https://doi.org/10.1038/s41561-021-00714-3

Burbank, D.W., Leland, J., Fielding, E., Anderson, R.S., Brozovic, N., Reid, M.R., et al. (1996) Bedrock incision, rock uplift and threshold hillslopes in the northwestern Himalayas. *Nature*, 379(6565), 505–510. Available from: https://doi.org/10.1038/379505a0

Burt, T.P., Adamson, J.K. & Lane, A.M.J. (1998) Long-term rainfall and streamflow records for north Central England: putting the environmental change network site at moor house, upper Teesdale, in context. *Hydrological Sciences Journal*, 43(5), 775–787. Available from: https://doi.org/10.1080/02626669809492172

Chatanantavet, P. & Parker, G. (2009) Physically based modeling of bedrock incision by abrasion, plucking, and macroabrasion. *Journal of Geophysical Research - Earth Surface*, 114(F4), F04018. Available from: https://doi.org/10.1029/2008JF001044

Covington, M.D., Gulley, J.D. & Gabrovšek, F. (2015) Natural variations in calcite dissolution rates in streams: controls, implications, and open questions. *Geophysical Research Letters*, 42(8), 2836–2843. Available from: https://doi.org/10.1002/2015GL063044

Covington, M.D. & Vaughn, K.A. (2019) Carbon dioxide and dissolution rate dynamics within a karst underflow-overflow system, Savoy experimental watershed, Arkansas, USA. *Chemical Geology*, 527, 118689. Available from: https://doi.org/10.1016/j.chemgeo.2018.03.009

Emberson, R., Hovius, N., Galy, A. & Marc, O. (2016) Chemical weathering in active mountain belts controlled by stochastic bedrock landsliding. *Nature Geoscience*, 9(1), 42–45. Available from: https://doi.org/10.1038/ngeo2600

Ferguson, R.I., Sharma, B.P., Hardy, R.J., Hodge, R.A. & Warburton, J. (2017) Flow resistance and hydraulic geometry in contrasting reaches of a bedrock channel. *Water Resources Research*, 53(3), 2278–2293. Available from: https://doi.org/10.1002/2016WR020233

Ferguson, R.I., Sharma, B.P., Hodge, R.A., Hardy, R.J. & Warburton, J. (2017) Bed load tracer mobility in a mixed bedrock/alluvial channel. *Journal of Geophysical Research - Earth Surface*, 122(4), 807–822. Available from: https://doi.org/10.1002/2016JF003946

Finnegan, N.J., Sklar, L.S. & Fuller, T.K. (2007) Interplay of sediment supply, river incision, and channel morphology revealed by the transient evolution of an experimental bedrock channel. *Journal of Geophysical Research - Earth Surface*, 112(F3), F03S11. Available from: https://doi.org/10.1029/2006JF000569

Ford, D. & Williams, P.D. (2007) *Karst hydrogeology and geomorphology*. John Wiley & Sons.

Fox, M., Hoseason, T., Bernard, T., Sinclair, H. & Smith, A.G.G. (2023) Bedload-bedrock contrasts form enigmatic low-relief surfaces of the Pyrenees. *Geophysical Research Letters*, 50(6), e2022GL101995. Available from: https://doi.org/10.1029/2022GL101995

Giachetta, E., Refice, A., Capolongo, D., Gasparini, N.M. & Pazzaglia, F.J. (2014) Orogen-scale drainage network evolution and response to erodibility changes: insights from numerical experiments. *Earth Surface Processes and Landforms*, 39(9), 1259–1268. Available from: https://doi.org/10.1002/esp.3579

Hancock, G.S., Small, E.E. & Wobus, C. (2011) Modeling the effects of weathering on bedrock-floored channel geometry. *Journal of Geophysical Research - Earth Surface*, 116(F3), F03018. Available from: https://doi.org/10.1029/2010JF001908

Howard, A.D. (1998) Long Profile Development of Bedrock Channels: Interaction of Weathering, Mass Wasting, Bed Erosion, and Sediment Transport. In: Tinkler, K.J. & Wohl, E. (Eds.) *Rivers over rock: fluvial processes in bedrock channels*. American Geophysical Union, pp. 297–319 https://doi.org/10.1029/GM107p0297

Huda, S.A. & Small, E.E. (2014) Modeling the effects of bed topography on fluvial bedrock erosion by saltating bed load. *Journal of Geophysical Research - Earth Surface*, 119(6), 1222–1239. Available from: https://doi.org/10.1002/2013JF002872

Hurst, M.D., Mudd, S.M., Attal, M. & Hilley, G. (2013) Hillslopes record the growth and decay of landscapes. *Science*, 341(6148), 868–871. Available from: https://doi.org/10.1126/science.1241791

Johnson, G.A.L. & Dunham, K.C. (1963) *The geology of Moor House*. Monographs of the Nature Conservancy, No. 002. Her Majesty's Stationery Office.

Johnson, K.N. & Finnegan, N.J. (2015) A lithologic control on active meandering in bedrock channels. *GSA Bulletin*, 127(11-12), 1766–1776. Available from: https://doi.org/10.1130/B31184.1

Kent, E., Whittaker, A.C., Boulton, S.J. & Alçiçek, M.C. (2020) Quantifying the competing influences of lithology and throw rate on bedrock river incision. *GSA Bulletin*, 133(7-8), 1649–1664. Available from: https://doi.org/10.1130/B35783.1

Lamb, M.P., Finnegan, N.J., Scheingross, J.S., & Sklar, L.S., (2015). New insights into the mechanics of fluvial bedrock erosion through flume experiments and theory. Geomorphology, Laboratory Experiments in Geomorphology 46th Annual Binghamton Geomorphology Symposium 18–20 September 2015 244, 33–55. https://doi.org/10.1016/j.geomorph.2015.03.003

Larimer, J.E., Yager, E.M., Yanites, B.J. & Witsil, A.J. (2021) Flume experiments on the erosive energy of bed load impacts on rough and planar beds. *Journal of Geophysical Research: Earth Surface*, 126(4), e2020JF005834. Available from: https://doi.org/10.1029/2020JF005834

Larimer, J.E., Yanites, B.J. & Jung, S.J. (2022) A field study on the lithological influence on the interaction between weathering and abrasion processes in bedrock Rivers. *Journal of Geophysical Research - Earth Surface*, 127(4), e2021JF006418. Available from: https://doi.org/10.1029/2021JF006418

Li, T., Venditti, J.G. & Sklar, L.S. (2023) Steady-state Bedrock Channel width. *Geophysical Research Letters*, 50(21), e2023GL105344. Available from: https://doi.org/10.1029/2023GL105344

Lifton, Z.M., Thackray, G.D., Van Kirk, R. & Glenn, N.F. (2009) Influence of rock strength on the valley morphometry of big creek, Central Idaho, USA. *Geomorphology*, 111(3-4), 173–181. Available from: https://doi.org/10.1016/j.geomorph.2009.04.014

Limaye, A.B.S. & Lamb, M.P. (2014) Numerical simulations of bedrock valley evolution by meandering rivers with variable bank material. *Journal of Geophysical Research - Earth Surface*, 119(4), 927–950. Available from: https://doi.org/10.1002/2013JF002997

Montgomery, D.R. (2004) Observations on the role of lithology in strath terrace formation and bedrock channel width. *American Journal of Science*, 304(5), 454–476. Available from: https://doi.org/10.2475/ajs.304.5.454

Morales, T., Uribe-Etxebarria, G., Uriarte, J.A. & Fernández de Valderrama, I. (2004) Geomechanical characterisation of rock masses in Alpine regions: the Basque arc (Basque-Cantabrian basin, northern Spain). *Engineering Geology*, 71(3-4), 343–362. Available from: https://doi.org/10.1016/S0013-7952(03)00160-1

Murphy, B.P., Johnson, J.P.L., Gasparini, N.M., Hancock, G.S. & Small, E.E. (2018) Weathering and abrasion of bedrock streambed topography. *Geology*, 46(5), 459–462. Available from: https://doi.org/10.1130/G40186.1

Murphy, B.P., Johnson, J.P.L., Gasparini, N.M. & Sklar, L.S. (2016) Chemical weathering as a mechanism for the climatic control of bedrock river incision. *Nature*, 532(7598), 223–227. Available from: https://doi.org/10.1038/nature17449

Nicholson, D.T. (2008) Rock control on microweathering of bedrock surfaces in a periglacial environment. *Geomorphology*, 101(4), 655–665. Available from: https://doi.org/10.1016/j.geomorph.2008.03.009

Nicholson, D.T. (2009) Holocene microweathering rates and processes on ice-eroded bedrock, Røldal area, Hardangervidda, southern Norway. *Geological Society of London, Special Publication*, 320(1), 29–49. Available from: https://doi.org/10.1144/SP320.3

Opdyke, B.N., Gust, G. & Ledwell, J.R. (1987) Mass transfer from smooth alabaster surfaces in turbulent flows. *Geophysical Research Letters*, 14(11), 1131–1134. Available from: https://doi.org/10.1029/GL014i011p01131

Ott, R.F., Gallen, S.F., Caves Rugenstein, J.K., Ivy-Ochs, S., Helman, D., Fassoulas, C., et al. (2019) Chemical versus mechanical denudation in meta-clastic and carbonate bedrock catchments on crete, Greece, and mechanisms for steep and high carbonate topography. *Journal of Geophysical Research: Earth Surface*, 124(12), 2943–2961. Portico. Available from: https://doi.org/10.1029/2019jf005142

Palmer, A.N. (1991) Origin and morphology of limestone caves. *GSA Bulletin*, 103(1), 1–21. Available from: https://doi.org/10.1130/0016-7606(1991)103<0001:OAMOLC>2.3.CO;2

Phillips, J.D., Pawlik, Ł. & Šamonil, P. (2019) Weathering fronts. *Earth-Science Reviews*, 198, 102925. Available from: https://doi.org/10.1016/j.earscirev.2019.102925

Rennie, S.; Adamson, J.; Anderson, R.; Andrews, C.; Bater, J.; Bayfield, N.; Beaton, K.; Beaumont, D.; Benham, S.; Bowmaker, V.; Britt, C.; Brooker, R.; Brooks, D.; Brunt, J.; Common, G.; Cooper, R.; Corbett, S.; Critchley, N.; Dennis, P.; Dick, J.; Dodd, B.; Dodd, N.; Donovan, N.; Easter, J.; Flexen, M.; Gardiner, A.; Hamilton, D.; Hargreaves, P.; Hatton-Ellis, M.; Howe, M.; Kahl, J.; Lane, M.; Langan, S.; Lloyd, D.; McCarney, B.; McElarney, Y.; McKenna, C.; McMillan, S.; Milne, F.; Milne, L.; Morecroft, M.; Murphy, M.; Nelson, A.; Nicholson, H.; Pallett, D.; Parry, D.; Pearce, I.; Pozsgai, G.; Rose, R.; Schafer, S.; Scott, T.; Sherrin, L.; Shortall, C.; Smith, R.; Smith, P.; Tait, R.; Taylor, C.; Taylor, M.; Thurlow, M.; Turner, A.; Tyson, K.; Watson, H.; Whittaker, M.; Wood, C. (2017). *UK environmental change network (ECN) stream water chemistry data: 1992-2015*. NERC Environmental Information Data Centre. https://doi.org/10.5285/fd7ca5ef-460a-463c-ad2b-5ad48bb4e22e

Scheingross, J.S., Brun, F., Lo, D.Y., Omerdin, K. & Lamb, M.P. (2014) Experimental evidence for fluvial bedrock incision by suspended and bedload sediment. *Geology*, 42(6), 523–526. Available from: https://doi.org/10.1130/G35432.1

Schlunegger, F., Melzer, J. & Tucker, G. (2001) Climate, exposed source-rock lithologies, crustal uplift and surface erosion: a theoretical analysis calibrated with data from the Alps/North Alpine Foreland Basin system. *International Journal of Earth Sciences*, 90(3), 484–499. Available from: https://doi.org/10.1007/s005310100174

Sharma, B.P. (2016) *Sediment dynamics in a Bedrock Channel* (PhD Thesis). Durham University. Available at: http://etheses.dur.ac.uk/11942/

Shennan, I. (1989) Holocene crustal movements and sea-level changes in Great Britain. *Journal of Quaternary Science*, 4(1), 77–89. Available from: https://doi.org/10.1002/jqs.3390040109

Shobe, C.M., Hancock, G.S., Eppes, M.C. & Small, E.E. (2017) Field evidence for the influence of weathering on rock erodibility and channel form in bedrock rivers. *Earth Surface Processes and Landforms*, 42(13), 1997–2012. Available from: https://doi.org/10.1002/esp.4163

Sklar, L.S. & Dietrich, W.E. (2001) Sediment and rock strength controls on river incision into bedrock. *Geology*, 29(12), 1087–1090. Available from: https://doi.org/10.1130/0091-7613(2001)029<1087:SARSCO>2.0.CO;2

Sklar, L.S. & Dietrich, W.E. (2004) A mechanistic model for river incision into bedrock by saltating bed load. *Water Resources Research*, 40(6). Portico. Available from: https://doi.org/10.1029/2003wr002496

Small, E.E., Blom, T., Hancock, G.S., Hynek, B.M. & Wobus, C.W. (2015) Variability of rock erodibility in bedrock-floored stream channels based on abrasion mill experiments. *Journal of Geophysical Research - Earth Surface*, 120(8), 1455–1469. Available from: https://doi.org/10.1002/2015JF003506

Spotila, J.A., Moskey, K.A. & Prince, P.S. (2015) Geologic controls on bedrock channel width in large, slowly-eroding catchments: case study of the New River in eastern North America. *Geomorphology*, 230, 51–63. Available from: https://doi.org/10.1016/j.geomorph.2014.11.004

Turowski, J.M., Pruß, G., Voigtländer, A., Ludwig, A., Landgraf, A., Kober, F., et al. (2023) Geotechnical controls on erodibility in fluvial impact erosion. *Earth Surface Dynamics*, 11(5), 979–994. Available from: https://doi.org/10.5194/esurf-11-979-2023

Viles, H., Goudie, A., Grab, S. & Lalley, J. (2011) The use of the Schmidt hammer and Equotip for rock hardness assessment in geomorphology and heritage science: a comparative analysis. *Earth Surface Processes and Landforms*, 36(3), 320–333. Available from: https://doi.org/10.1002/esp.2040

West, A.J., Galy, A. & Bickle, M. (2005) Tectonic and climatic controls on silicate weathering. *Earth and Planetary Science Letters*, 235(1-2), 211–228. Available from: https://doi.org/10.1016/j.epsl.2005.03.020

Whipple, K.X. (2004) Bedrock Rivers and the geomorphology of active Orogens. *Annual Review of Earth and Planetary Sciences*, 32(1), 151–185. Available from: https://doi.org/10.1146/annurev.earth.32.101802.120356

Whipple, K.X., Hancock, G.S. & Anderson, R.S. (2000) River incision into bedrock: mechanics and relative efficacy of plucking, abrasion, and cavitation. *GSA Bulletin*, 112(3), 490–503. Available from: https://doi.org/10.1130/0016-7606(2000)112<490:RIIBMA>2.0.CO;2

Yanites, B.J. & Tucker, G.E. (2010) Controls and limits on bedrock channel geometry. *Journal of Geophysical Research - Earth Surface*, 115(F4), F04019. Available from: https://doi.org/10.1029/2009JF001601

SUPPORTING INFORMATION

Additional supporting information can be found online in the Supporting Information section at the end of this article.

How to cite this article: Dingle, E.H., Baynes, E.R.C., Hall, A. & Warburton, J. (2025) Erosion dynamics in carbonate bedrock channels inhibit weathering processes. *Earth Surface Processes and Landforms*, 50(5), e70067. Available from: https://doi.org/10.1002/esp.70067